01 Feb 2003

Temperature Dependence of Droplet Nucleation in a Yukawa Fluid

Jinsong Li

Gerald Wilemski
Missouri University of Science and Technology, wilemski@mst.edu

Recommended Citation

J. Li and G. Wilemski, "Temperature Dependence of Droplet Nucleation in a Yukawa Fluid," *Journal of Chemical Physics*, vol. 118, no. 6, pp. 2845-2852, American Institute of Physics (AIP), Feb 2003.
The definitive version is available at https://doi.org/10.1063/1.1534830

Temperature dependence of droplet nucleation in a Yukawa fluid

Jin-Song Li[a] and Gerald Wilemski[b]
Department of Physics and Cloud and Aerosol Sciences Laboratory, University of Missouri-Rolla, Rolla, Missouri 65409-0640

(Received 15 August 2002; accepted 11 November 2002)

We have studied the temperature dependence of gas-to-liquid nucleation in Yukawa fluids with gradient theory and density functional theory. Each of these nonclassical theories exhibits a weaker (i.e., better) temperature dependence than classical nucleation theory. At fixed temperature, the reversible work to form a critical nucleus found from gradient theory approaches the value given by density functional theory as the supersaturation increases. At high temperatures, the two theories remain quite close over a wide range of vapor densities. As the temperature is reduced, the difference between the two theories increases with decreasing vapor density. Compared to the classical theory we find that gradient theory can improve the predicted temperature dependence of the nucleation rate, although not always to the same degree as density functional theory. Finally, our results show that the scaling behavior of density functional theory proposed by McGraw and Laaksonen can be extended to higher temperatures if the incompressibility assumption is avoided when evaluating the classical reversible work. © *2003 American Institute of Physics.*
[DOI: 10.1063/1.1534830]

I. INTRODUCTION

In recent years there has been considerable interest in the density functional theory of nucleation.[1–16] Density functional theory (DFT) is a rigorous statistical mechanical approach in which the free energy of an inhomogeneous system is expressed as a functional of the system's density profile. The correct density profile extremizes this free energy functional, and with this profile, various thermodynamic properties of the system may readily be calculated. DFT is appealing because its use of interparticle potentials allows the effects of molecular interactions on the nucleation process to be directly included in the calculations. However, applications to real substances require accurate intermolecular potentials. This greatly complicates the application of DFT to some of the most interesting substances used in experiments, such as water or hydrocarbons,[11] since their potentials are very complex or even unavailable.

Gradient theory (GT) is the simplest approximate form of DFT. Gradient theory was first devised by van der Waals[17] using intuitive arguments and was independently redeveloped much later by Cahn and Hilliard.[18] Since then, it has been the subject of much scrutiny and application.[19–28] Originally, this theory was expected to hold only in the critical region. It appears, however, that at least qualitatively the theory also gives good results close to the triple point.[26,28,29] An attractive feature of GT is that the homogeneous term in the free energy density can be derived from an equation of state (EOS). Hence, it is possible to apply GT to substances composed of polar or nonspherical molecules, such as water or hydrocarbons, which are more difficult to treat with DFT. Although GT is much easier to use than DFT, an important question to resolve is how much accuracy is sacrificed by using GT versus DFT. Thus, it is necessary to compare GT with the less approximate form of DFT for various systems.

Zeng and Oxtoby[2] have shown that for the Lennard-Jones potential, DFT produces a temperature dependence for the ratio of nonclassical to classical nucleation rate, J_{NC}/J_C, that is very close to experimental observations for various systems.[30,31] Iwamatsu and Horii have found a similar result for the Yukawa fluid.[6] Recently, Barrett[9] has compared GT and a semiempirical form[5] of DFT for nonane nucleation. He found that although the DFT results did not reproduce the experimental trend, they did improve the predicted temperature dependence of the nucleation rate. However, the GT results showed almost the same temperature dependence as the classical theory and, moreover, depended on the specific EOS used. Gráńasy has reported similarly disappointing results for GT.[8] A fair amount of empiricism is necessarily involved in the GT calculations, and although the approaches taken in Refs. 8 and 9 are quite reasonable, it is at least a possibility that the EOS used and the method of parameter evaluation may have adversely affected the GT results in each case. In this paper, we further explore this question. However, we do not revisit the calculations of Barrett and Gráńasy, which are certainly valid in their own right. Rather, we make extensive calculations with GT and DFT for the hard sphere–Yukawa fluid using the properties of this fluid as determined by DFT to parametrize the GT calculations. This approach should afford GT its best chance of reproducing the results of its more rigorous cousin. We use the Yukawa system because of its relative computational simplicity and because it is known to give a realistic temperature dependence for the nucleation rate.[6] Also, the Yukawa and Lennard-Jones potentials produce very similar results when used in the semiempirical DFT of Nyquist *et al.*[5]

[a]Electronic mail: jsli@umr.edu
[b]Electronic mail: wilemski@umr.edu

II. THEORY

A. Density functional theory

We consider a one component nonuniform system without external fields in which a liquid nucleus is formed within the gas phase. Treating the attractive forces as a perturbation in a hard sphere reference fluid, the Helmholtz free energy for this system can be written as[1]

$$F[\rho(\mathbf{r})]=\int d\mathbf{r} f_h[\rho(\mathbf{r})] + \frac{1}{2}\int d\mathbf{r}\int d\mathbf{r}'\rho(\mathbf{r})\rho(\mathbf{r}')w(|\mathbf{r}-\mathbf{r}'|), \quad (1)$$

where $\rho(\mathbf{r})$ is the number density at point $\mathbf{r}$, $f_h(\rho)$ is the Helmholtz free energy per unit volume of a uniform hard sphere fluid of density ρ, and w is the attractive part of the pair potential. The grand potential has the form[1]

$$\Omega[\rho(\mathbf{r})]=F[\rho(\mathbf{r})]-\mu_B\int d\mathbf{r}\rho(\mathbf{r}), \quad (2)$$

where μ_B is chemical potential of the bulk vapor phase.

The hard sphere Helmholtz free energy density is given by

$$f_h(\rho)=\rho\mu_h(\rho)-p_h(\rho), \quad (3)$$

where μ_h and p_h are the local chemical potential and pressure of the hard-sphere fluid, respectively. By employing the Carnahan–Starling[32] results, μ_h and p_h can be represented as

$$\mu_h(\eta)=kT\left[\ln\eta+\frac{(8\eta-9\eta^2+3\eta^3)}{(1-\eta)^3}\right], \quad (4)$$

$$p_h(\rho)=kT\rho\frac{1+\eta+\eta^2-\eta^3}{(1-\eta)^3}. \quad (5)$$

Here, k is Boltzmann's constant, T is the temperature, and η is the packing fraction, $\eta=\pi\sigma^3\rho/6$, where σ is the hard sphere diameter. To complete the model, the attractive pair potential must be specified. Here, we choose the potential to have the Yukawa form,

$$w(r)=-\alpha\lambda^3\exp(-\lambda r)/4\pi\lambda r, \quad (6)$$

where λ is the range parameter and $\alpha=-\int d\mathbf{r}w(\mathbf{r})$.

The system density profile $\rho(\mathbf{r})$ is obtained from the variational condition,

$$\delta\Omega[\rho(\mathbf{r})]/\delta\rho(\mathbf{r})=0, \quad (7)$$

which leads to an integral Euler equation[1]

$$\mu_h[\rho(\mathbf{r})]=\mu_B-\int d\mathbf{r}'\rho(\mathbf{r}')w(|\mathbf{r}-\mathbf{r}'|). \quad (8)$$

For the spherically symmetric Yukawa potential, ρ is only a function of the radial variable r, and Eq. (8) reduces to a one-dimensional equation, which can be differentiated twice with respect to r to obtain the differential equation[4,6]

$$d^2[r\mu_h(r)]/dr^2=r\lambda^2[\mu_0(\rho)-\mu_B], \quad (9)$$

where μ_0 is the chemical potential of the homogeneous fluid at density ρ,

$$\mu_0(\rho)=\mu_h(\rho)-\alpha\rho(r). \quad (10)$$

To obtain droplet density profiles, this equation is solved numerically for $\mu_h(r)$ with the boundary conditions for a spherical interface,

$$\frac{d\mu_h(r)}{dr}\to 0, \quad \text{when } r\to 0,$$

$$\mu_h(r)\to\mu_h|_{\rho=\rho_B}, \quad \text{when } r\to\infty,$$

where ρ_B is the density of the bulk vapor phase. The corresponding density profile is determined by inverting Eq. (4).

The reversible work W to form a nucleus is the difference between the grand potentials for the nonuniform system, Eq. (2), and the initial uniform system, $(-p_BV)$,

$$W=\int d\mathbf{r}\{f_h[\rho(r)]-\mu_B\rho(r)+p_B\} + \frac{1}{2}\int d\mathbf{r}\int d\mathbf{r}'\rho(r)\rho(r')w(|\mathbf{r}-\mathbf{r}'|), \quad (11)$$

where p_B is the pressure of bulk vapor phase. This equation can be simplified by employing Eqs. (3) and (8) to find

$$W=\int d\mathbf{r}[\tfrac{1}{2}\rho(r)[\mu_h(\rho)-\mu_B]+p_B-p_h(\rho)]. \quad (12)$$

In this form, W is readily determined once the solutions for $\rho(r)$ and $\mu_h(\rho)$ have been found.

B. Gradient theory

Gradient theory employs a Helmholz free-energy density that consists of the homogeneous fluid contribution plus an inhomogeneous term that is proportional to the square of the local density gradient. The total Helmholtz free energy F of an inhomogeneous system is the integral of the Helmholtz free energy density f over the volume of the system

$$F=\int f(\rho)d\mathbf{r}, \quad (13)$$

where f is given by[25,26]

$$f(\rho)=f_0(\rho)+\frac{c}{2}(\nabla\rho)^2, \quad (14)$$

for a closed one-component system without external fields. Here, $f_0(\rho)$ is the Helmholtz free energy density of the homogeneous fluid at the local density $\rho(r)$, $\nabla\rho(r)$ is the local density gradient, and c is the influence parameter. Since c depends only weakly on density, it can be regarded as constant at a given temperature.[25]

The equilibrium density profile $\rho(r)$, corresponding to an extremum of the free energy functional, is determined by the Euler equation[25]

$$\mu_B=\mu_0(\rho)-c\nabla^2\rho(r), \quad (15)$$

where $\mu_0\equiv\partial f_0/\partial\rho$ is the chemical potential of the homogeneous fluid at density ρ.

For a uniform hard sphere–Yukawa fluid of density ρ, the pressure is given by

$$p(\rho)=p_h(\rho)-\tfrac{1}{2}\alpha\rho^2. \quad (16)$$

The corresponding Helmholtz-free energy density of the homogeneous fluid is

$$f_0(\rho)=f_h(\rho)-\tfrac{1}{2}\alpha\rho^2=\rho\mu_0(\rho)-p(\rho), \tag{17}$$

where

$$f_h(\rho)=\rho kT(\ln\eta-1)+\rho kT\frac{\eta(4-3\eta)}{(1-\eta)^2}, \tag{18}$$

and the chemical potential $\mu_0(\rho)$ is given by Eq. (10).

The reversible work equals the difference between the free energy of a system containing a drop and that of a homogeneous system at the same temperature, volume, and with the same number of molecules. Hence, the reversible work can be expressed as

$$W=\int[f(\rho)-f_0(\rho^0)]d\mathbf{r}, \tag{19}$$

where $f_0(\rho^0)\equiv\rho^0\mu^0-p^0$ is the Helmholtz free energy density of the initial uniform gas phase. The final conditions of the gas phase, ρ_B and p_B, differ from the initial conditions of the system, ρ^0 and p^0. However, the differences are very small when the system is very large, and we may expand $f_0(\rho^0)$ in terms of the bulk gas density ρ_B and pressure p_B, i.e.,

$$\mu_0(p^0)=\mu_0(p_B)+\left.\frac{\partial\mu_0}{\partial p}\right|_{p_B}(p^0-p_B)+\cdots. \tag{20}$$

Since $\partial\mu_0/\partial p=1/\rho$ holds, we have

$$f_0(\rho^0)=\rho_B\mu_B-p_B+\mu_B(\rho^0-\rho_B)+(\rho^0-\rho_B)(p^0-p_B)/\rho_B+\cdots, \tag{21}$$

where $\mu_B=\mu_0(p_B)$. After we neglect the small second order term in Eq. (21) and substitute Eqs. (14) and (21) into Eq. (19), we find for W the following result first obtained by Cahn and Hilliard:[19]

$$W=\int\left[\Delta\omega+\frac{c}{2}|\nabla\rho|^2\right]d\mathbf{r}, \tag{22}$$

where

$$\Delta\omega=\omega(\rho)-\omega(\rho_B), \tag{23}$$

$$\omega(\rho)\equiv f_0(\rho)-\rho\mu_B, \tag{24}$$

and the condition of conservation of molecules

$$\int(\rho-\rho^0)d\mathbf{r}=0, \tag{25}$$

has been used. It is not hard to show that Eqs. (12) and (22) are formally identical. This requires an integration by parts of the square gradient term in Eq. (22) and the use of Eqs. (10), and (15)–(17). Thus, Eq. (12) may be used to calculate W for either theory by using the appropriate density profile.

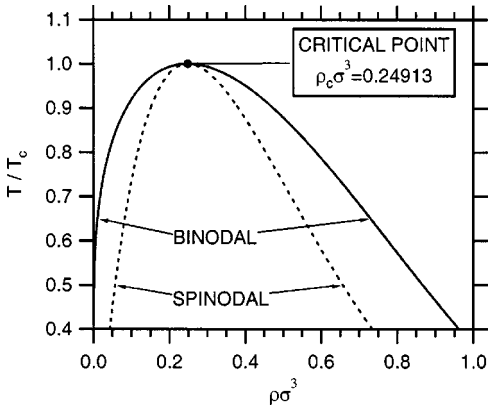

FIG. 1. Phase diagram for the hard sphere–Yukawa fluid based on the mean field equation of state.

III. BULK PROPERTIES AND PLANAR SURFACE TENSION

A. Phase diagram

The coexisting densities of bulk liquid ρ_l and vapor ρ_v are determined by solving the simultaneous equations

$$\mu_0(T,\rho_l)=\mu_0(T,\rho_v), \tag{26}$$

$$p(T,\rho_l)=p(T,\rho_v). \tag{27}$$

The liquid and vapor spinodal densities, ρ_{ls} and ρ_{vs}, respectively, are determined by solving the equation,

$$\frac{d\mu_0}{d\rho}=0, \tag{28}$$

at fixed T. By employing Eqs. (10) and (16), we found the phase diagram for the hard sphere–Yukawa fluid shown in Fig. 1. As noted in Ref. 1, the attractive force parameter α in these equations is related to the critical temperature T_c by the expression $\alpha=11.102kT_c\sigma^3$.

B. Density functional theory

The equilibrium properties of a planar interface are determined by the one-dimensional analog of Eq. (9),

$$\frac{d^2\mu_h(x)}{dx^2}=\lambda^2[\mu_0(\rho)-\mu], \tag{29}$$

where μ is the equilibrium chemical potential and x the distance normal to the interface. With the aid of the thermodynamic identity, $\rho(d\mu_h)_T=(dp_h)_T$, a first integral[33] of Eq. (29) is readily found to be

$$\left[\frac{d\mu_h(x)}{\lambda dx}\right]^2=[\mu_h(x)-\mu]^2-2\alpha[p_h(\rho)-p]. \tag{30}$$

This equation can be numerically integrated to obtain the density profile.

The surface tension of a planar interface can be obtained from[4,34]

$$\gamma_\infty=\frac{1}{\alpha\lambda^2}\int_{-\infty}^{\infty}[\mu_h'(x)]^2dx=\frac{1}{\alpha\lambda^2}\int_{\mu_h^V}^{\mu_h^L}|\mu_h'|d\mu_h, \tag{31}$$

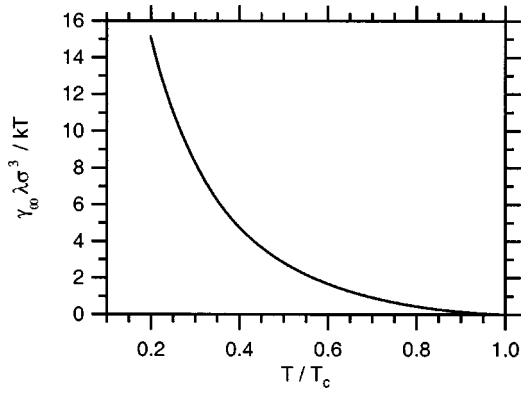

FIG. 2. Surface tension of the planar vapor–liquid interface of the hard sphere–Yukawa system calculated with density functional theory as a function of temperature.

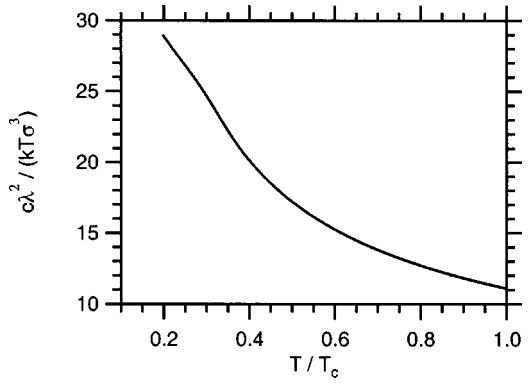

FIG. 3. Dimensionless influence parameter as a function of temperature.

where $\mu_h' = d\mu_h/dx$ is defined by Eq. (30). Using Eq. (30), Eq. (31) can be reduced to

$$\gamma_\infty = \frac{1}{\alpha\lambda}\int_{\rho_v}^{\rho_l} [(\mu_h(\rho)-\mu)^2 - 2\alpha(p_h(\rho)-p)]^{1/2}\left(\frac{d\mu_h}{d\rho}\right) d\rho. \tag{32}$$

Thus, we can obtain the surface tension of a planar interface without knowing the density profile. The surface tension calculated from Eq. (32) is shown in Fig. 2 as a function of T.

C. Gradient theory

The equilibrium density profile of a planar interface is determined by the one-dimensional version of Eq. (15),

$$c\frac{d^2\rho(x)}{dx^2} = \mu_0(\rho) - \mu. \tag{33}$$

In this case, a first integral for Eq. (33) is

$$\left[\frac{d\rho(x)}{dx}\right]^2 = 2[\omega(\rho) - \omega(\rho_v)]/c, \tag{34}$$

where ω is defined by Eq. (24). The surface tension γ_∞ of the planar interface can be calculated directly from the influence parameter c and the thermodynamic function, $\omega(\rho)$, of the homogeneous system using the equation[23,35]

$$\gamma_\infty = \int_{\rho_v}^{\rho_l} \sqrt{2c[\omega(\rho) - \omega(\rho_v)]}\, d\rho. \tag{35}$$

The above equation gives us an empirical way to determine the influence parameter c for real systems by requiring that the surface tension calculated from Eq. (35) equal the experimentally measured value. For the hard sphere–Yukawa system, we determine the parameter c from the surface tension determined by Eq. (32). Figure 3 shows the results. Once c is determined, we can obtain the density profiles of the planar interface for GT. Figure 4 shows the planar interfaces predicted by Eqs. (30) and (34). At high temperature, the GT density profiles are very close to those from DFT. Our DFT profile at $T/T_c = 0.8$ is in good agreement with Hadjiagapiou's.[4] For low temperatures, the DFT density profiles are visibly sharper on the vapor side, but the GT profiles are slightly sharper on the liquid side.

IV. SPHERICAL INTERFACE

A. Numerical technique

Equations (9) and (15) are similar in structure. Each can be solved numerically with an iterative technique that uses a Newton–Raphson approach to assist convergence. Critical to the Newton–Raphson method is that the initial trial solution must be accurate enough to fall within the domain of convergence.[36] Since droplets are large at low supersaturations, curvature effects are small, and the density profile approaches that of a planar liquid–vapor interface at the same temperature. Thus, the density profile of the planar interface is the most common initial guess.

To solve the two differential Eqs. (9) and (15), we first introduce the following dimensionless variables: density, $\tilde{\rho} = \rho\sigma^3$; chemical potential, $\tilde{\mu} = \mu/kT$, length (DFT), $\tilde{r} = \lambda r$; and length (GT), $\tilde{r} = \lambda r/\sqrt{\tilde{c}}$, where $\tilde{c}$ is the dimensionless influence parameter $\tilde{c} = c\lambda^2/(kT\sigma^3)$. In terms of these variables, Eqs. (9) and (15) now appear as

$$d^2g/d\tilde{r}^2 = \tilde{r}[\tilde{\mu}_0(\tilde{\rho}) - \tilde{\mu}_B], \tag{36}$$

where $g(\tilde{r}) = \tilde{r}n$ and n denotes $\tilde{\mu}_h$ for DFT and $\tilde{\rho}$ for GT.

We then use a finite-difference scheme over a domain of $N+1$ equally spaced mesh points, so that $\tilde{r} = ih$, where

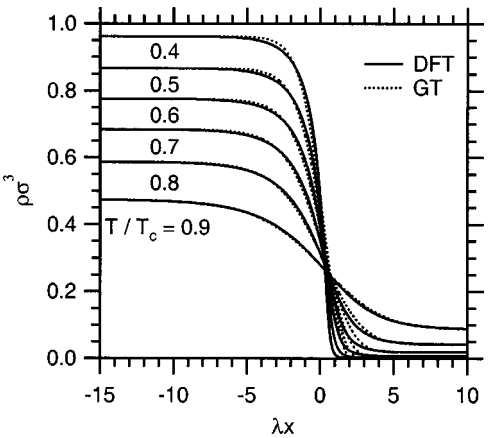

FIG. 4. Density profiles for planar vapor–liquid interfaces of the Yukawa system for density functional theory (DFT) and gradient theory (GT) at various reduced temperatures.

$i(=0,\ldots,N)$ is the mesh point index and h is the dimensionless step size. After approximating $\tilde{\mu}_0(\tilde{\rho})$ by its first order Taylor expansion and using central differences for all derivatives, we put Eq. (36) into the following finite-difference form,

$$6n_1^{k+1}+\left(6+h^2\left[\frac{d\tilde{\mu}_0}{dn}\right]_{n=n_0^k}\right)n_0^{k+1} =h^2\left(\tilde{\mu}_0(n_0^k)-\tilde{\mu}_B-n_0^k\left[\frac{d\tilde{\mu}_0}{dn}\right]_{n=n_0^k}\right) \quad (i=0), \tag{37}$$

$$g_{i+1}^{k+1}-\left(h^2\left[\frac{d\tilde{\mu}_0}{dn}\right]_{n=n_i^k}+2\right)g_i^{k+1}+g_{i-1}^{k+1} =ih^3\left(\tilde{\mu}_0(n_i^k)-\tilde{\mu}_B-n_i^k\left[\frac{d\tilde{\mu}_0}{dn}\right]_{n=n_i^k}\right) \quad (i=1,\ldots,N), \tag{38}$$

where n_0 is the value of n at the drop center, and $n_{N+1}=n_B$. The subscript "i" labels the mesh points, and superscript "k" denotes the iteration number. Note that by using the dimensionless length $\tilde{r}$ and density $\tilde{\rho}$, these numerical density profiles depend only on the choice made for α, but not on specific values for λ or σ. Thermodynamic properties, such as the surface tension and the reversible work, scale in simple ways[1,6] with λ and σ, and results for particular values are easily found from the dimensionless results presented below.

The iterative solution process begins by using the initial trial profile for all n_i^0 values in Eqs. (37) and (38). The equations are solved using a standard tridiagonal matrix routine.[36] This solution then serves as the next trial profile. The iteration procedure is terminated when the difference between successive iterates becomes less than a prescribed limit Δ, i.e., when

$$\Sigma\equiv\left(\sum_{i=0}^{N}|\tilde{\rho}_i^{k+1}-\tilde{\rho}_i^k|^2\right)^{1/2}<\Delta. \tag{39}$$

For our DFT calculations, typical parameter values are $N=10^5$, $h=4\times10^{-4}$, and $\Delta=4.0\times10^{-8}$ when the vapor density is not very high. (For the GT calculations, h is reduced by the additional scaling factor $\sqrt{\tilde{c}}$.) When ρ_B is close to the spinodal value ($\rho_s-\rho_B\lesssim10^{-1}\rho_s$), the density profile is very flat and decays very slowly to the bulk value. To accurately capture this slow decay, we must substantially enlarge the spatial domain in which the profile is determined. To do this without incurring substantial computational costs, we took advantage of the profile's flatness and simply increased h by a factor of 25. The flatness of the profile near the spinodal also means that the profile can be found more accurately there. So, for example, converged profiles can be found for $\Delta=5.0\times10^{-9}$ near the spinodal, but farther from the spinodal, this degree of accuracy cannot be attained. Once the first density profile is obtained, the density profiles of smaller drops can be found easily by using the converged profile at the previous ρ_B value as the trial guess. We compared results obtained in the forward direction (from low ρ_B to high ρ_B) with those in the backward direction (from high ρ_B to low ρ_B), to verify that our solutions were unique. For both GT and DFT, it takes only 5–6 steps to reach convergence, and, thereafter, Σ only fluctuates in a very small range. We ran test cases for as many as 500 iterations, and the profile always remained stable. The mean value of Σ for DFT is slightly higher than that for GT, because of the extra step to convert μ_h to ρ. In contrast to the integral equation approach,[1] this method of solution for DFT appears to be stable when applied to unstable as well as equilibrium fluid states.

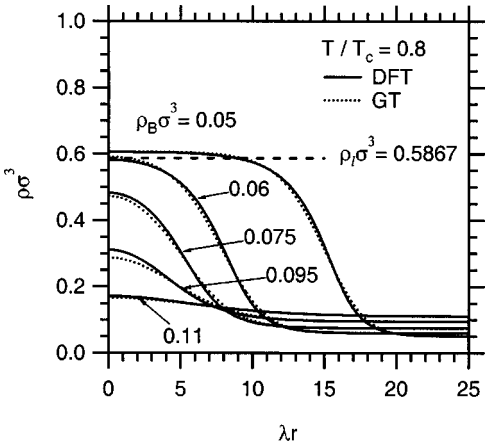

FIG. 5. Density profiles of critical droplets at various values of the bulk vapor density for DFT and GT at the reduced temperature $T/T_c=0.8$. Also indicated is the reduced bulk liquid density $\rho_l\sigma^3$.

B. Results for spherical droplets

We have compared our DFT results with those previously published. Our density profiles are in excellent agreement with those reported by Oxtoby and Evans[1] at $T/T_c=0.6$ and by Iwamatsu and Horii[6] at $T/T_c=0.7$, but the density profiles of Hadjiagapiou[4] at $T/T_c=0.8$ differ considerably from ours. Hadjiagapiou provides no details on the numerical method used to calculate the density profiles, so we are unable to comment further on this discrepancy. Figures 5 and 6 show several of the density profiles we obtained by solving Eqs. (9) and (15) for different values of ρ_B at $T/T_c=0.8$ and at $T/T_c=0.5$. For low vapor densities, the results for the two theories are very close. With increasing ρ_B, some deviations appear near the center of the drop, but disappear as ρ_B approaches the spinodal value. The deviations in the density profiles are magnified at lower temperatures. Gránásy has found similar behavior for nonane density profiles.[8]

Figure 7 shows the reversible work W for these two models for $T/T_c=0.4$, 0.6, 0.8, and 0.9. These results, as well as those in the following figures, are given in terms of the dimensionless quantity $W(\lambda\sigma)^3/kT$, which is the natural scaling that follows from Eq. (12) after introducing dimensionless variables. Our results at $T/T_c=0.6$ are in excellent agreement with those calculated by Oxtoby and Evans.[1] GT

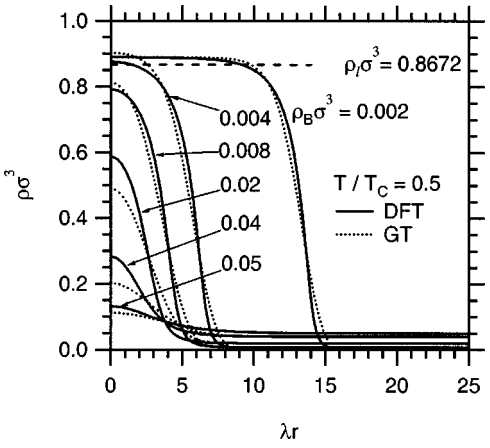

FIG. 6. Same as Fig. 5 but at the reduced temperature $T/T_c=0.5$.

and DFT give very close results at high supersaturations, but deviations appear as the supersaturation is lowered. The deviations are also larger at lower temperatures. Also shown in the figure is the classical reversible work W_C. This is calculated by approximating Gibbs'[37] original formula through the use of the bulk surface tension to give,

$$W_C=\frac{16\pi}{3}\frac{\gamma_\infty^3}{(\Delta p)^2}\ , \tag{40}$$

where $\Delta p=p(\rho_l^R)-p(\rho_B)$ and $p(\rho_l^R)$ is the pressure of a bulk liquid phase (the reference phase) of density ρ_l^R whose chemical potential is the same as the bulk gas phase,[37–39] i.e.,

$$\mu_0(T,\rho_B)=\mu_0(T,\rho_l^R). \tag{41}$$

As shown in Fig. 7, the gradient theory does provide a considerable improvement over the classical nucleation theory.

The improvement over classical theory is shown in another way in Fig. 8, where we plot the difference $\Delta W=W_C-W_{NC}$ in reversible work between each of the nonclassical theories and the classical nucleation theory. At high temperatures, the difference for DFT monotonically decays with decreasing density ρ_B, but at $T/T_c=0.5$ an inflection point has

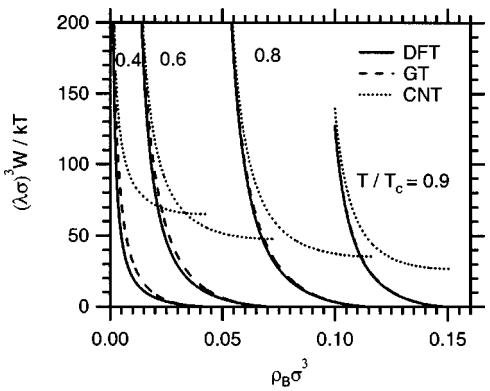

FIG. 7. Reversible work of critical droplet formation as a function of the reduced bulk vapor density $\rho_B\sigma^3$ at four reduced temperatures. Results are for density functional theory (DFT), gradient theory (GT), and classical nucleation theory, Eq. (40), (CNT). For clarity, curves for only four reduced temperatures are shown. Each curve terminates at the spinodal vapor density; values are listed in the Fig. 8 caption.

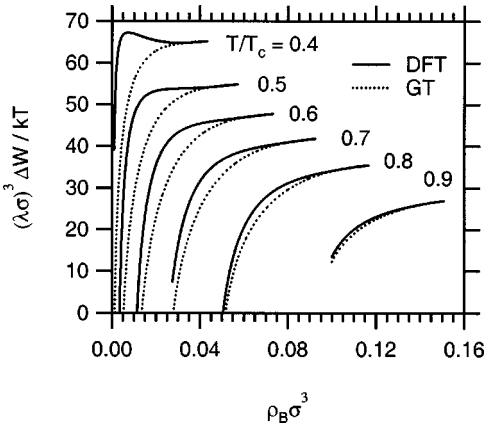

FIG. 8. The difference $(\Delta W=W_C-W_{NC})$ between the nonclassical work of droplet formation and the classical value given by Eq. (40) as a function of reduced bulk vapor density at six reduced temperatures. Each curve terminates at the spinodal density: $\rho_s\sigma^3=0.04312$, 0.05711, 0.07325, 0.09248, 0.1167, 0.1508, respectively, in order of increasing temperature.

appeared. At $T/T_c=0.4$, the inflection point has developed into a shallow minimum and a maximum located quite far from the spinodal. In contrast, the difference for GT shows a monotonic decay with decreasing density ρ_B at all temperatures. Although we do not show it, it should be noted that each of the ΔW curves goes negative, i.e., $W_{NC}>W_C$, at small enough densities before eventually returning to zero at the coexistence density. Similar behavior was previously noted by Oxtoby and Evans[1] and Iwamatsu and Horii[6] for the Yukawa system and by Koga and Xeng[12] for the Lennard-Jones system. The high density region of each curve is usually considered to be more relevant because there the nucleation barriers will be low and the corresponding nucleation rates can reach observable magnitudes. Although the curves are strictly never flat at high densities, each one has a range over which ΔW changes slowly with decreasing density. As Iwamatsu and Horii[6] and McGraw and Laaksonen[7] have previously noted, in these approximately flat regions the nonclassical theories behave in accordance with the experimental observation that the correct reversible work differs from the classical value by a temperature dependent constant. We can examine this behavior in another way by plotting W_{NC} vs W_C for each nonclassical theory. This is shown in Fig. 9. As previously found by Iwamatsu and Horii,[6] over the range of physically most relevant values ($W<80kT$) the DFT results lie on lines that are approximately parallel and whose distance from the $W_{NC}=W_C$ line increases as T is lowered. The GT results show similar behavior only at the higher temperatures, $T/T_c=0.8$, 0.9; for $T/T_c\leqslant 0.7$ the GT results are not parallel to the $W_{NC}=W_C$ line except in the high density region whose size is minimized in the plot because W_C does not vary greatly in this density range.

Figure 10 is similar to Fig. 9, but here the comparison is with a different approximate form of the classical reversible work W_C^a that is widely used in the nucleation field since, unlike Eq. (40), it does not usually require knowledge of the fluid EOS for its evaluation. By assuming an incompressible liquid nucleus of bulk density ρ_l we find the approximate relationship $\Delta p=\rho_l\Delta\mu$, where $\Delta\mu=\mu_0(T,\rho_B)-\mu_0(T,\rho_l)$

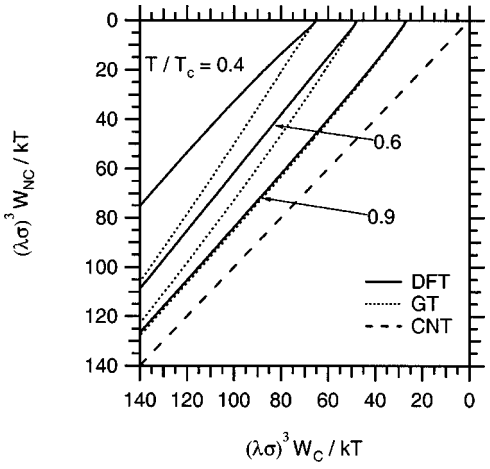

FIG. 9. Nonclassical reversible work of droplet formation W vs the classical value W_C (CNT) as given by Eq. (40). For clarity, results are shown at only three reduced temperatures.

is the difference in the chemical potential between the metastable and equilibrium states. It then follows from Eq. (40) that

$$W_C^a = \frac{16\pi}{3} \frac{\gamma_\infty^3}{(\rho_l \Delta\mu)^2}. \tag{42}$$

Koga and Xeng[12] have also shown that W_C^a is essentially[40] the leading term in an expansion of Gibbs' formally exact result for W in powers of $\Delta\mu$. Our interest in this form stems from its role in the scaling analysis of McGraw and Laaksonen,[7] who found for the Lennard-Jones fluid that

$$W_{\mathrm{DFT}} = W_C^a - D(T), \tag{43}$$

where $D(T)$ is a temperature dependent constant. We see from the results in Fig. 10 that for the Yukawa fluid the scaling behavior given by Eq. (43) does not hold for $T/T_c \geqslant 0.8$, but should be satisfactory below this temperature. Since the maximum temperature considered by McGraw and Laaksonen was about $T/T_c = 0.74$, the validity of this scaling

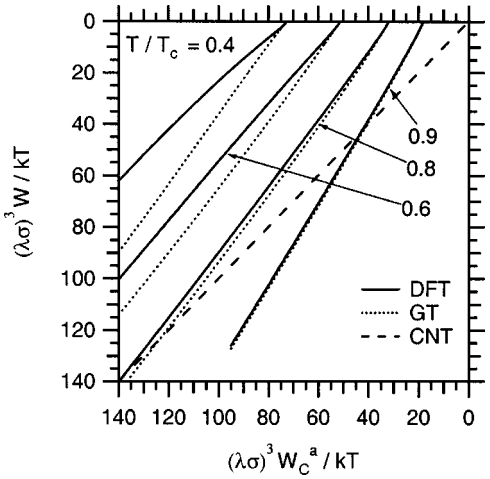

FIG. 10. Nonclassical reversible work of droplet formation W vs the classical value W_C^a (CNT) as given by Eq. (42). For clarity, results are shown at only four reduced temperatures.

behavior in the Lennard-Jones system at higher temperatures is unknown. The differences between Figs. 9 and 10 must result from the inadequacy of the incompressibility assumption at higher temperatures. The lack of parallelism implies that classical theory in the form of Eq. (42) will disagree strongly with either DFT or GT in describing the supersaturation dependence of the nucleation rate at high temperature. Thus, the less approximate form W_C given by Eq. (40) is preferred since it provides the basis for a more general scaling behavior of the form proposed by McGraw and Laaksonen and predicts the same supersaturation dependence as DFT at all temperatures.

V. CONCLUSIONS

We have studied the temperature dependence of critical droplet formation for a Yukawa fluid with two versions of density functional theory. From our results we draw the following conclusions:

(1) The gradient theory results are close to those of the more rigorous density functional theory when either temperature or supersaturation is high.
(2) Compared to the classical theory, gradient theory does improve the temperature dependence of the nucleation rate. At high temperatures, the degree of improvement over a wide vapor density range is almost the same as that of density functional theory. Less improvement is found when the temperature and supersaturation are low.
(3) The scaling relations of McGraw and Laaksonen[7] may be extended to a wider range of conditions by avoiding the incompressibility assumption in determining the classical reversible work of nucleus formation.

ACKNOWLEDGMENTS

The authors thank B. E. Wyslouzil for helpful comments on our manuscript. G.W. thanks R. Strey and B. Rathke for interesting discussions about the results of this paper. This work was supported by the Engineering Physics Program of the Division of Materials Sciences and Engineering, Basic Energy Sciences, U.S. Department of Energy.

[1] D. W. Oxtoby and R. Evans, J. Chem. Phys. **89**, 7521 (1988).
[2] X. C. Zeng and D. W. Oxtoby, J. Chem. Phys. **94**, 4472 (1991).
[3] V. Talanquer and D. W. Oxtoby, J. Chem. Phys. **100**, 5190 (1994).
[4] I. Hadjiagapiou, J. Phys.: Condens. Matter **6**, 5303 (1994).
[5] R. M. Nyquist, V. Talanquer, and D. W. Oxtoby, J. Chem. Phys. **103**, 1175 (1995).
[6] M. Iwamatsu and K. Horii, J. Non-Cryst. Solids **205–207**, 919 (1996).
[7] R. McGraw and A. Laaksonen, Phys. Rev. Lett. **76**, 2754 (1996).
[8] L. Gránásy, J. Non-Cryst. Solids **219**, 49 (1997).
[9] J. C. Barrett, J. Phys.: Condens. Matter **9**, L19 (1997).
[10] V. Talanquer, J. Chem. Phys. **106**, 9957 (1997).
[11] C. Seok and D. W. Oxtoby, J. Chem. Phys. **109**, 7982 (1998).
[12] K. Koga, and X. C. Zeng, J. Chem. Phys. **110**, 3466 (1999).
[13] J. C. Barrett, J. Chem. Phys. **111**, 5938 (1999).
[14] L. Gránásy and D. W. Oxtoby, J. Chem. Phys. **112**, 2399 (2000).
[15] V. K. Shen and P. G. Debenedetti, J. Chem. Phys. **114**, 4149 (2001).
[16] I. Napari and A. Laaksonen, J. Chem. Phys. **114**, 5796 (2001).
[17] J. D. van der Waals, Verh.-K. Ned. Akad. Wet., Afd. Natuurkd., Reeks Eerste **1**, 1 (1893).
[18] J. W. Cahn and J. E. Hilliard, J. Chem. Phys. **28**, 258 (1958).

[19] J. W. Cahn and J. E. Hilliard, J. Chem. Phys. **31**, 688 (1959).
[20] A. J. M. Yang, P. D. Fleming III, and J. H. Gibbs, J. Chem. Phys. **64**, 3732 (1976).
[21] P. D. Fleming III, A. J. M. Yang, and J. H. Gibbs, J. Chem. Phys. **65**, 7 (1976).
[22] V. Bongiorno and H. T. Davis, Phys. Rev. A **12**, 2213 (1976).
[23] B. S. Carey, L. E. Scriven, and H. T. Davis, AIChE J. **24**, 1076 (1978).
[24] B. S. Carey, L. E. Scriven, and H. T. Davis, AIChE J. **26**, 705 (1980).
[25] A. H. Falls, L. E. Scriven, and H. T. Davis, J. Chem. Phys. **75**, 3986 (1981).
[26] H. T. Davis and L. E. Scriven, Adv. Chem. Phys. **49**, 357 (1982).
[27] P. M. W. Cornelisse, C. J. Peters, and J. de Swaan Arons, J. Chem. Phys. **106**, 9820 (1997).
[28] L. Gránásy, J. Chem. Phys. **109**, 9660 (1998).
[29] M. M. Telo da Gama and R. Evans, Mol. Phys. **38**, 367 (1979).
[30] C. Hung, M. J. Krasnopoler, and J. L. Katz, J. Chem. Phys. **90**, 1856 (1989).
[31] Y. Viisanen and R. Strey, J. Chem. Phys. **101**, 7835 (1994).
[32] N. F. Carnahan and K. E. Starling, J. Chem. Phys. **51**, 635 (1969).
[33] D. E. Sullivan, Phys. Rev. B **20**, 3991 (1979).
[34] D. E. Sullivan, J. Chem. Phys. **74**, 2604 (1981).
[35] H. T. Davis, *Statistical Mechanics of Phases, Interfaces, and Thin Films* (VCH, New York, 1996).
[36] W. H. Press, B. P. Flannery, S. A. Teukolsky, and W. T. Vetterling, *Numerical Recipes: The Art of Scientific Computing* (Cambridge University Press, Cambridge, England, 1985).
[37] J. W. Gibbs, Trans. Conn. Acad. Arts Sci. **3**, 343 (1878), reprinted in *The Scientific Papers of J. W. Gibbs* (Dover, New York, 1961), Vol. I.
[38] K. Nishioka, Metall. Trans. A **23A**, 1896 (1992).
[39] J.-S. Li and K. Nishioka, J. Cryst. Growth **171**, 259 (1996).
[40] The exact form of the leading term is $(16\pi/3)\gamma_\infty^3/(\Delta\rho\Delta\mu)^2$, where $\Delta\rho$ is the difference in the densities of the bulk equilibrium phases. At low enough temperatures, where $\Delta\rho \simeq \rho_l$, Eq. (42) is recovered.